Neuron, Vol. 41, 929–942, March 25, 2004, Copyright ©2004 by Cell Press

Fusion Pore Dynamics Are Regulated by Synaptotagmin•t-SNARE Interactions

Jihong Bai, Chih-Tien Wang, David A. Richards, Meyer B. Jackson, and Edwin R. Chapman*
Department of Physiology
University of Wisconsin
Madison, Wisconsin 53706

Summary

Exocytosis involves the formation of a fusion pore that connects the lumen of secretory vesicles with the extracellular space. Exocytosis from neurons and neuroendocrine cells is tightly regulated by intracellular [Ca^{2+}] and occurs rapidly, but the molecular events that mediate the opening and subsequent dilation of fusion pores remain to be determined. A putative Ca^{2+} sensor for release, synaptotagmin I (syt), binds directly to syntaxin and SNAP-25, which are components of a conserved membrane fusion complex. Here, we show that Ca^{2+}-triggered syt•SNAP-25 interactions occur rapidly. The tandem C2 domains of syt cooperate to mediate binding to syntaxin/SNAP-25; lengthening the linker that connects C2A and C2B selectively disrupts this interaction. Expression of the linker mutants in PC12 cells results in graded reductions in the stability of fusion pores. Thus, the final step of Ca^{2+}-triggered exocytosis is regulated, at least in part, by direct contacts between syt and SNAP-25/syntaxin.

Introduction

Neurotransmitter release from nerve terminals is initiated by Ca^{2+} (Katz, 1969) and is mediated by the fusion of synaptic vesicles with the presynaptic plasma membrane. The entire process of release is completed in an extremely short time frame (i.e., micro- to milliseconds) (Llinas et al., 1981; Sabatini and Regehr, 1996). Thus, Ca^{2+}-triggered exocytotic membrane fusion can involve only a handful of molecular rearrangements. These restrictions imply direct interactions between the Ca^{2+} sensor(s) and the membrane fusion machinery at a late step in secretion (Augustine, 2001; Chapman, 2002).

A set of proteins, termed soluble NSF (*N*-ethylmaleimide-sensitive fusion factor) attachment protein receptors (SNAREs), play essential roles in most, and perhaps all, intracellular membrane fusion events (Ferro-Novick and Jahn, 1994; Rothman, 1994). These proteins can be divided into two categories: target membrane SNAREs (t-SNAREs), including syntaxin and synaptosome-associated protein of 25 kDa (SNAP-25); and the vesicle SNARE (v-SNARE) synaptobrevin (also known as vesicle-associated membrane protein, VAMP). The cytoplasmic domains of SNARE proteins assemble into a four-helix bundle (Sutton et al., 1998) that can mediate membrane fusion by pulling the vesicle and target membranes together (Weber et al., 1998). However, in order for the SNARE complex to drive rapid membrane fusion in response to Ca^{2+} influx, additional factors, including a Ca^{2+} sensor(s), are required.

The secretory vesicle protein, synaptotagmin I (syt), is thought to function as a major Ca^{2+} sensing protein that regulates neurotransmitter release (Augustine, 2001; Chapman, 2002). Syt is anchored to the vesicle membrane via a single membrane-spanning domain near its N terminus (Perin et al., 1990); the cytoplasmic domain is composed of two Ca^{2+} binding modules called C2 domains (Brose et al., 1992; Davletov and Sudhof, 1993; Desai et al., 2000; Fernandez et al., 2001). The N-terminal C2 domain (C2A) and C-terminal C2 domain (C2B) are tethered together by a short flexible linker composed of nine residues (Sutton et al., 1999). Genetic and acute perturbation studies revealed that syt is essential for evoked neurotransmitter release (Bommert et al., 1993; DiAntonio et al., 1993; Geppert et al., 1994; Littleton et al., 1993; Nonet et al., 1993) and suggest that the Ca^{2+} binding abilities of each C2 domain play roles in the Ca^{2+}-triggered fusion of docked vesicles (Fernandez-Chacon et al., 2001; Littleton et al., 2001; Mackler et al., 2002; Robinson et al., 2002; Stevens and Sullivan, 2003; but see also Fernandez-Chacon et al., 2002).

Biochemical studies led to the identification of a number of Ca^{2+}-dependent syt-effector interactions that might couple Ca^{2+} influx to fusion (Augustine, 2001; Chapman, 2002), including syt•membrane interactions (Bai et al., 2002; Brose et al., 1992), syt•syt oligomerization (Wu et al., 2003), and syt•t-SNARE interactions (Chapman et al., 1995; Schiavo et al., 1997).

While direct interactions between syt and t-SNAREs provides a compelling connection between the putative Ca^{2+} sensor and the fusion apparatus, the physiological relevance of this interaction is unclear. Reagents that block the interaction of syt with syntaxin and SNAP-25 (Earles et al., 2001; Tucker et al., 2003) or mutations in SNAP-25 that disrupt interactions with syt (Zhang et al., 2002) reduce secretion. Using purified SNAREs reconstituted into proteoliposomes, syt stimulated membrane fusion by facilitating SNARE complex formation (Mahal et al., 2002). These findings support a model in which syt functions during fusion at least in part by interacting with SNARE proteins. However, there are no data to indicate whether syt•t-SNARE interactions function during the final steps of fusion, i.e., the opening and dilation of fusion pores. Indeed, in vitro assays suggest that syt•t-SNARE interactions may function to mediate vesicle docking prior to fusion (Chieregatti et al., 2002).

Here, we have addressed the question of whether Ca^{2+}-triggered binding of syt to SNAP-25 is fast enough to mediate excitation-secretion coupling. Moreover, we have generated a series of mutant syts with selective and graded losses in SNAP-25/syntaxin binding activity and assessed their impact on the kinetic properties of fusion pores. Our data suggest that rapid Ca^{2+}-triggered syt•t-SNARE interactions control fusion pore dynamics during the final steps of exocytosis.

*Correspondence: chapman@physiology.wisc.edu

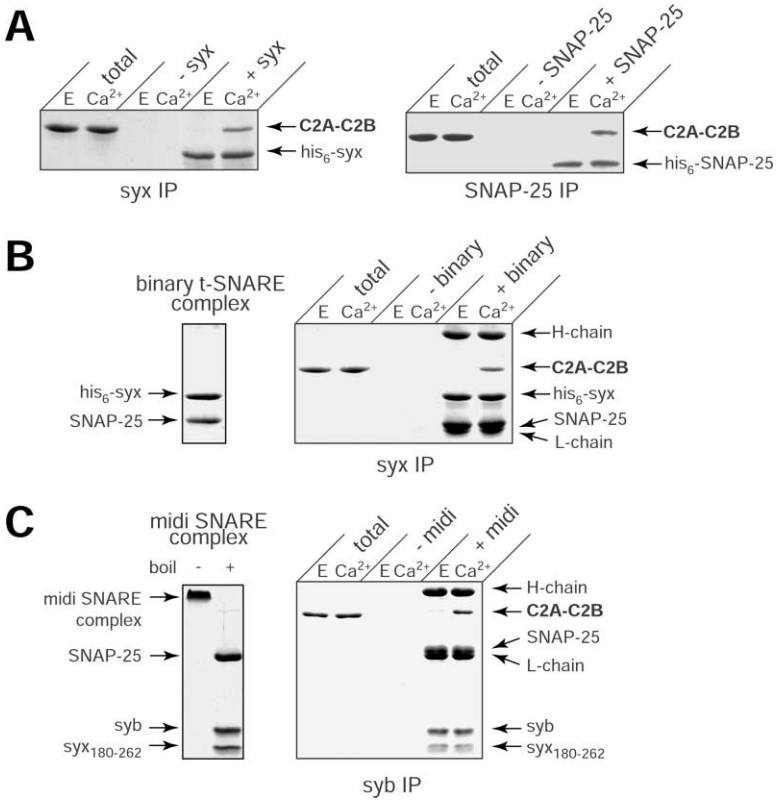

Figure 1. Ca^{2+} Triggers Binding of the Cytoplasmic Domain of syt to Isolated t-SNAREs, t-SNARE Heterodimers, and Assembled SNARE Complexes

Co-immunoprecipitation experiments were carried out as described in Experimental Procedures. 30% of the bound material was loaded onto the gel and separated by SDS-PAGE; bands were visualized with Coomassie blue. Total corresponds to 10% of the binding reaction. Controls lacking t-SNAREs and antibodies were analyzed in parallel.

(A) C2A-C2B binds to syntaxin (syx; left) and SNAP-25 (right) in a Ca^{2+}-dependent manner. C2A-C2B (2 μM) was incubated either with or without full-length his_6-syntaxin or his_6-SNAP-25 (2 μM) in the presence of 2 mM EGTA or 1 mM Ca^{2+} in 150 μl TBS. Syntaxin was immunoprecipitated with monoclonal antibody HPC-1; SNAP-25 was immunoprecipitated with monoclonal antibody 71.2.

(B) C2A-C2B binds to syntaxin/SNAP-25 heterodimers in a Ca^{2+}-dependent manner. Purified t-SNARE heterodimers are shown at left. Co-immunoprecipitation of C2A-C2B with syntaxin/SNAP-25 heterodimers (right) was carried out using HPC-1 as described in (A).

(C) Ca^{2+}-dependent binding of C2A-C2B to assembled SNARE complexes. Experiments were carried out as in (A), except that C2A-C2B was mixed with assembled SDS-resistant midi SNARE complexes (2 μM; left), and co-immunoprecipitation (right) was carried out using an anti-syb monoclonal antibody (69.1).

Results

Ca^{2+} Triggers Direct Interactions between syt and t-SNAREs at All Stages of SNARE Complex Assembly

Current evidence suggests that the assembly of *trans* SNARE complexes functions to pull lipid bilayers together to mediate fusion (Weber et al., 1998). A key unresolved question is when, relative to the Ca^{2+} trigger, *trans* SNARE complexes are formed. Structural studies indicate that syntaxin and SNAP-25 first assemble into heterodimers, followed by the binding of synaptobrevin (syb), resulting in formation of a four-helix bundle (Fiebig et al., 1999; Sutton et al., 1998). At present, most data are consistent with the idea that Ca^{2+} triggers the final zippering together of SNARE complexes and thereby drives fusion (Chen et al., 1999).

Previous studies established that Ca^{2+} promotes direct interactions between syt and both SNAP-25 and syntaxin (e.g., Chapman et al., 1995; Gerona et al., 2000). In the first series of experiments we compared, side by side, the ability of the cytoplasmic domain of syt (C2A-C2B) to bind syntaxin (Figure 1A, left), SNAP-25 (Figure 1A, right), SNAP-25/syntaxin heterodimers (Figure 1B), and fully assembled "midi" SNARE complexes (composed of full-length SNAP-25, the cytoplasmic domain of synaptobrevin II, and residues 180–262 of syntaxin 1A) (Figure 1C). In all cases, little binding was observed in the absence of Ca^{2+}, but stoichiometric binding was observed upon addition of Ca^{2+}. We conclude that syt can engage t-SNAREs at all stages of SNARE complex assembly. Since synaptobrevin assembles with t-SNAREs after they first assemble into heterodimers, and because the fully assembled SNARE complex may not form until after fusion, the most likely targets of Ca^{2+}•syt during exocytosis are isolated t-SNAREs and/or SNAP-25/syntaxin heterodimers.

Kinetics of syt•SNAP-25 Interactions

A key question that has been raised is whether Ca^{2+}-triggered syt•t-SNARE interactions occur rapidly enough to couple Ca^{2+} influx to fusion (Hilfiker et al., 1999). To address this issue, we developed a FRET assay to monitor the time course of syt•SNAP-25 interactions. Trp residues in C2A-C2B served as energy donors, and AEDANS acceptors were covalently bound to four Cys residues in SNAP-25. We found that at the relatively high concentrations needed for these studies, C2A-C2B•SNAP-25 complexes tend to form insoluble aggregates in response to Ca^{2+} (unpublished observations). To overcome this problem, we used a mutant version of C2A-C2B (K326,327A, designated as C2A-C2B*) that does not aggregate under the conditions of the kinetics experiments. The lysine mutations reduce t-SNARE binding activity (Rickman et al., 2004), but quantitative analysis reveals that the stoichiometry of binding is unaffected and that these mutations only shift the Kd from 3 μM to 10 μM (Figure 4A, see Supplemental Figure S1 at http://www.neuron.org/cgi/content/full/41/6/929/DC1).

As expected, addition of Ca^{2+} to the AEDANS-SNAP-25•C2A-C2B* mixture triggered an increase in the intensity of the AEDANS signal from SNAP-25 (Figure 2A) and a decrease in the Trp fluorescence of C2A-C2B* (data not shown). The observed signal changes were

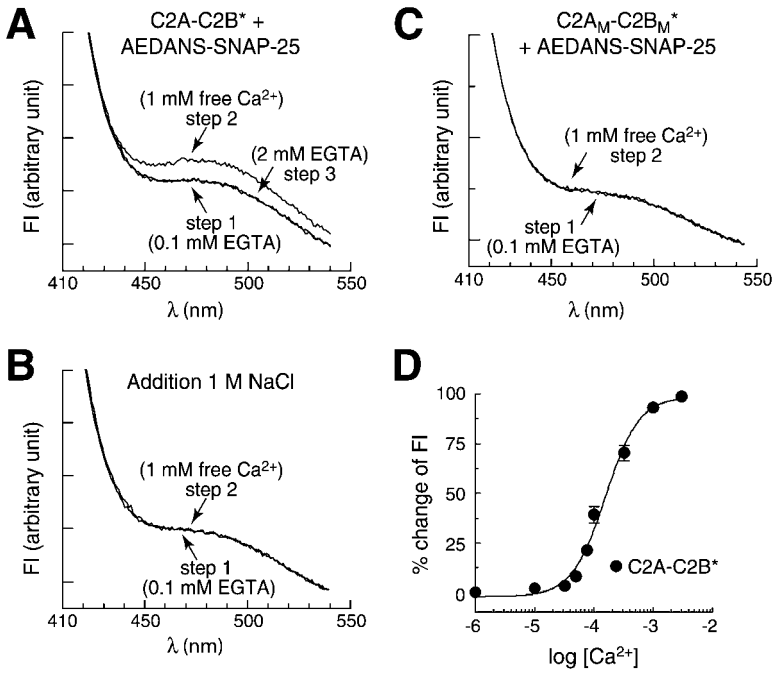

Figure 2. FRET Reports Ca^{2+}-Dependent and Reversible Interactions between syt and SNAP-25

(A) Native Trp residues (amino acids 259, 390, and 404) in C2A-C2B* (the asterisk indicates the K326,327A mutation that prevents aggregation of syt•SNAP-25 complexes, as detailed in the text) served as the energy donors and were excited at 285 nm. The emission spectra of the AEDANS-SNAP-25 acceptor were collected from 420 to 540 nm. C2A-C2B* (10 μM) and AEDANS-SNAP-25 (1 μM) were mixed in the presence of 0.1 mM EGTA (step 1), Ca^{2+} was then added to reach a final Ca^{2+} concentration of 1 mM (step 2). Addition of Ca^{2+} triggered an increase in AEDANS fluorescence and a decrease in Trp fluorescence (data not shown). The increase in AEDANS fluorescence was reversed by adding 2 mM EGTA (step 3).

(B) C2A-C2B*•AEDANS-SNAP-25 interactions are sensitive to ionic strength. Experiments were carried out as described in (A) but in the presence of 1 M NaCl. The fluorescence intensity of the AEDANS acceptor was the same in EGTA and Ca^{2+}, indicating that C2A-C2B*•AEDANS-SNAP-25 interactions are abolished in buffers with high ionic strength.

(C) Ca^{2+} binding to C2A-C2B* is essential for the syt•SNAP-25 interactions observed using the FRET assay. Two Ca^{2+} ligands in each C2 domain of C2A-C2B* were neutralized (D230,232N in C2A and D363,365N in C2B) to disrupt Ca^{2+} binding (Fernandez et al., 2001; Zhang et al., 1998), Ca^{2+}-triggered membrane binding, and Ca^{2+}-triggered t-SNARE binding activities (Earles et al., 2001) of syt. This mutant version of C2A-C2B* failed to induce the Ca^{2+}-dependent increase in the AEDANS acceptor.

(D) Ca^{2+} dependence of C2A-C2B*•AEDANS-SNAP-25 complex assembly measured via FRET. The corrected emission spectra were obtained as described in (A) and integrated from 440 to 540 nm. The changes in fluorescence intensity were normalized, plotted, and fit as a function of $[Ca^{2+}]_{free}$ with GraphPad Prism 2.0 software. The $[Ca^{2+}]_{1/2}$ was 155 ± 15 μM and the Hill coefficient was 1.5 ± 0.2.

fully reversed by chelating Ca^{2+} with EGTA. Increasing the salt concentration blocked the Ca^{2+}-induced increase in AEDANS fluorescence (Figure 2B), indicating that binding of C2A-C2B* to AEDANS-SNAP-25 is mediated by electrostatic interactions. Neutralization of two acidic Ca^{2+} ligands in C2A and C2B also abolished the Ca^{2+}-triggered increase in AEDANS fluorescence (Figure 2C), ruling out the possibility that the FRET signal was reporting Ca^{2+}-triggered conformational changes in AEDANS-SNAP-25. The $[Ca^{2+}]_{1/2}$ for the FRET signal was 155 ± 15 μM (Figure 2D), which is identical to the $[Ca^{2+}]_{1/2}$ reported using bead pull-down assays (Gerona et al., 2000) and is similar to the Ca^{2+} dependence of syt•syntaxin interactions (Chapman et al., 1995). We note that the $[Ca^{2+}]_{1/2}$ for syt•t-SNARE interactions lies in the low μM range (<10 μM Ca^{2+}) in situ (Zhang et al., 2002). This is likely to be due to the presence of anionic lipids, which are known to increase the affinity of syt for Ca^{2+} (Brose et al., 1992).

Using FRET as a read-out, we found that C2A-C2B*•AEDANS-SNAP-25 complexes assembled and disassembled in response to changes in Ca^{2+} on timescales too rapid to resolve in manual mixing experiments. To obtain kinetic data on subsecond timescales, we used a stopped-flow rapid mixing approach. These experiments were carried out under conditions in which C2A-C2B* and AEDANS-SNAP-25 either were or were not premixed prior to addition of Ca^{2+}. The kinetics traces obtained under either condition were identical and revealed two distinct kinetic phases: a burst phase that was complete within the dead time of the instrument (1.2 ms) and a slower component that developed in ~10 ms (Figure 3A, top, and data not shown).

In parallel, we carried out co-immunoprecipitation experiments of C2A-C2B* and AEDANS-SNAP-25 under conditions identical to the stopped-flow experiments. Little binding was observed in EGTA, while robust binding was observed in the presence of Ca^{2+} (Figure 3A, lower panel). This observation, in conjunction with the identical kinetics traces obtained plus and minus preincubation, demonstrates that the rapid kinetic component of binding (complete in <1.2 ms) is due to Ca^{2+}-triggered interactions between C2A-C2B* and AEDANS-SNAP-25 rather than Ca^{2+}-triggered changes in preformed complexes. $C2A_M$-$C2B_M$*, which fails to bind Ca^{2+}, did not bind to SNAP-25 in the stopped-flow or co-immunoprecipitation assays (Figure 3B), further establishing that the FRET signal in Figures 2A and 3A is due to Ca^{2+}-triggered binding of C2A-C2B* to AEDANS-SNAP-25.

The dead time of stopped-flow experiments limits the observable reaction rates to <1000 s^{-1}. Assuming a Kd for C2A-C2B*•AEDANS-SNAP-25 of 10 μM (data not shown), we calculated that the lower limit for the on rate (k_{on}) is ~5 × 10^7 $M^{-1}s^{-1}$. Thus, complex assembly must occur faster than this limit. The maximum encounter rate set by diffusion provides an upper limit of ~7 × 10^9 $M^{-1}s^{-1}$ (Davis et al., 1999).

The slower component of the FRET signal was well fitted by a single exponential function, yielding a rate of

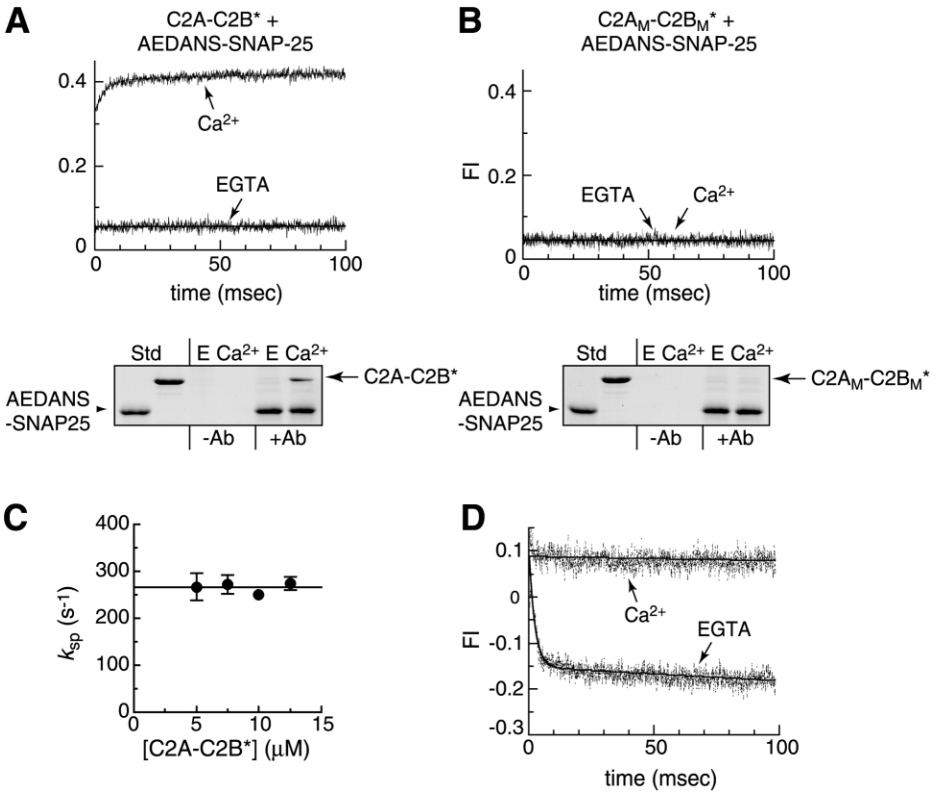

Figure 3. Rapid Ca^{2+}-Triggered Assembly and Rearrangements within C2A-C2B*•AEDANS-SNAP-25 Complexes

(A) Top: Ca^{2+}-dependent C2A-C2B*•AEDANS-SNAP-25 interactions exhibit at least two kinetic phases: a burst phase and a second slower phase. Stopped flow rapid mixing experiments were carried out under conditions in which the proteins were not premixed prior to addition of Ca^{2+}. The kinetics of a Ca^{2+}-triggered binding reaction are shown in the upper trace. As a control, a mixing experiment using 0.1 mM EGTA is shown the lower trace, thus providing a minimum reference point. The final [C2A-C2B*] was 10 μM and the final [AEDANS-SNAP-25] was 1 μM. The burst phase was complete within the dead time of the instrument (~1.2 ms), and the second phase could be fitted with a single exponential function (k_{sp} = 258 s^{-1}). Bottom: C2A-C2B* and AEDANS-SNAP-25 were mixed together under the same conditions as in the stopped-flow experiments and co-immunoprecipitated using 71.2 as described in Figure 1A.

(B) Neutralization of Ca^{2+} ligands in syt abolish Ca^{2+}-triggered interactions with SNAP-25. $C2A_M$-$C2B_M$* was generated as described in Experimental Procedures and analyzed for binding to AEDANS-SNAP-25 in the stopped-flow (top) and co-immunoprecipitation (bottom) assays as described in (A).

(C) The second kinetic component is due to conformational change(s) in the C2A-C2B*•AEDANS-SNAP-25 complex. Stopped-flow rapid mixing experiments were carried out as described in (A). k_{sp} was determined by fitting the data with single exponential functions and plotted versus [C2A-C2B*]. k_{sp} was not dependent on the concentration of C2A-C2B*, demonstrating that this kinetic component reflects postbinding conformational change(s) in the C2A-C2B*•AEDANS-SNAP-25 complex. Error bars represent standard deviations of k_{sp} values from 21 traces.

(D) Disassembly kinetics of Ca^{2+}•C2A-C2B*•AEDANS-SNAP-25 complexes upon chelation of Ca^{2+}. C2A-C2B*•AEDNS-SNAP-25 complexes were assembled at 500 μM Ca^{2+}. Disassembly reactions were carried out by rapidly mixing these complexes with 2 mM EGTA (final). Disassembly data were collected for 100 ms; the plot includes the best fit with a single exponential function (k_{diss} = 425 s^{-1}). As a control, samples were mixed with buffer containing 500 μM Ca^{2+}, providing a maximum signal reference.

258 s^{-1}. The rate of this phase was not dependent on [C2A-C2B*] (Figure 3C), demonstrating that this signal is reporting post binding conformational changes in the assembled complex, rather than association of C2A-C2B* with AEDANS-SNAP-25. This could reflect changes in the distance and/or orientation between the Trp donors and the AEDANS acceptor.

Finally, we observed that mixing C2A-C2B*•AEDANS-SNAP-25 complexes with excess Ca^{2+} chelator rapidly reversed the fluorescence increase (Figure 3D); the dissociation rate, k_{diss}, was 425 s^{-1}. These data demonstrate that Ca^{2+}-driven rearrangements in syt•t-SNARE complexes are fast enough to mediate excitation-secretion coupling (Bollmann et al., 2000; Llinas et al., 1981; Schneggenburger and Neher, 2000).

Selective Disruption of syt•t-SNARE Interactions

Our next goal was to selectively disrupt the t-SNARE binding activity of syt. Since neutralizing the Ca^{2+} binding sites in syt affects a number of Ca^{2+}-dependent interactions, we adopted a new strategy to diminish interactions with t-SNAREs. The rationale for this approach is shown in Figure 4. Syntaxin/SNAP-25 heterodimers were incubated with syt fragments in the presence and absence of Ca^{2+}, and the complexes were immunoprecipitated with antibodies directed against syntaxin. Consistent with previous results, Ca^{2+}-enhanced binding of C2A-C2B to t-SNARE heterodimers (Figure 4A, left); at saturation, binding approached 1 mole of C2A-C2B per mole of syntaxin (Figure 4A, right). As a control, syt was incubated with full-length synapto-

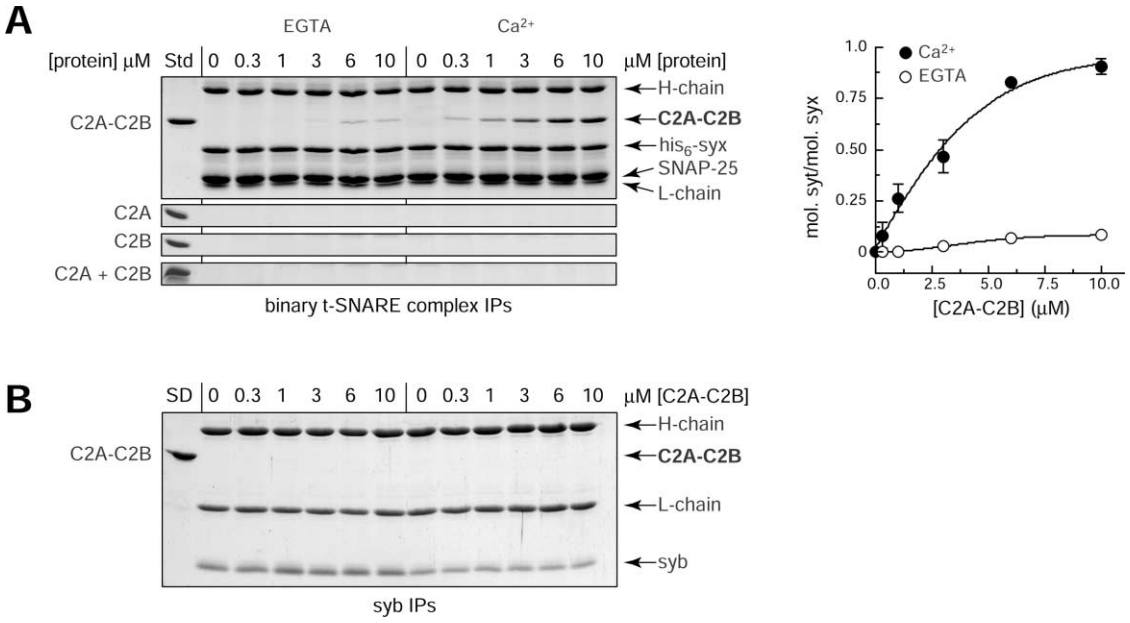

Figure 4. Both C2 Domains of syt Cooperate to Mediate Stiochiometric Binding to syntaxin/SNAP-25

(A) Left: The indicated C2A-C2B, C2A, or C2B (concentrations as indicated) were incubated with syntaxin/SNAP-25 heterodimers (2 μM) in 2 mM EGTA or 1 mM Ca^{2+}; samples were co-immunoprecipitated with HPC-1 and stained with Coomassie blue as described in Figure 1A. In the gel shown on the bottom, C2A and C2B were mixed together; the indicated concentration represents the concentration of each isolated C2 domain. Standards (Std) were 0.7 μg C2A-C2B and 0.45 μg C2A or C2B. Right: Binding of C2A-C2B to syntaxin was quantified by densitometry and is plotted versus [C2A-C2B]; at saturation the stoichiometry was 0.96:1. Syntaxin was used as the reference since the antibody light chain obscured the SNAP-25 band.

(B) C2A-C2B does not bind to full-length syb. Experiments were carried out as described in (A); syb was immunoprecipitated with 69.1.

brevin II; co-immunoprecipitation was not observed (Figure 4B).

While C2A-C2B forms stoichiometric complexes with syntaxin/SNAP-25 heterodimers, neither C2A nor C2B, alone or in combination, exhibited significant t-SNARE binding activity (Figure 4B). These results demonstrate that C2A and C2B must be tethered together in order for syt to bind tightly to syntaxin/SNAP-25 (Chapman et al., 1996). These findings indicate that if the linker were infinitely long, we would expect a loss of t-SNARE binding activity. According to this view, graded increases in the length of the linker would be expected to result in graded decreases in t-SNARE binding activity. We note that when isolated C2A-C2B or C2B are fused to GST, they can bind to t-SNAREs in a largely Ca^{2+}-independent manner (Tucker et al., 2003; Rickman et al., 2004), but this is an artifact due to the GST moiety (Tucker et al., 2003).

A schematic diagram of syt is shown in Figure 5A; the flexible linker that connects C2A and C2B is composed of nine residues. Elongation of the linker by inserting one copy (designated as 2×-linker) or two copies (designated as 3×-linker) of the linker sequence significantly reduced t-SNARE heterodimer binding activity (Figures 5B and 5C). Similar results were obtained using isolated t-SNAREs in bead pull-down experiments (data not shown) and in the FRET assay described above (Figure 5D), confirming that increases in the length of the linker results in decreased binding of syt to isolated SNAP-25 and syntaxin. We also carried out stopped flow rapid mixing experiments to study the effect of linker length on the speed of post binding conformational change in the C2A-C2B*•AEDANS-SNAP-25 complex. Doubling the linker length significantly slowed the second phase of signal change (Figure 5E; for C2A-C2B*, $k_{obs} = 250 \pm 6\ s^{-1}$; for 2×-linker*, $k_{obs} = 182 \pm 11\ s^{-1}$). Thus, the linker mutation also affects post binding Ca^{2+}-driven conformational changes in syt•SNAP-25 complexes.

To verify that the 2×- and 3×-linker mutations specifically disrupt interactions with t-SNAREs, a series of control experiments were carried out. Using ^{3}H-labeled liposome binding assays, we first determined whether the linker mutations affected the ability of syt to bind liposomes composed of PS (25%) and PC (75%). As shown in Figure 6A (left), the extent of PS/PC binding activity was not affected by the linker mutations.

A previous study established that the C2B domain of syt binds PS/PC liposomes with high affinity only when tethered to a C2A domain (Bai et al., 2002). This finding raises a concern that in the linker mutants, C2A may not be able to fully activate the adjacent C2B domain. To address this, we neutralized two Ca^{2+} binding residues in C2A (designated as $C2A_{2M}B$) and tested the Ca^{2+}-dependent membrane binding activity of C2B in the context of the cytoplasmic domain (Figure 6A, right). Under these conditions, all liposome binding activity is mediated solely by C2B (Bai et al., 2002). The results from this analysis demonstrate that lengthening the linker in C2A-C2B does not affect the ability of the C2B domain to engage PS/PC liposomes. Finally, the Ca^{2+} sensitivity of wild-type (wt) and linker mutant versions of C2A-C2B were identical (Figure 6B; $[Ca^{2+}]_{1/2}$ values were 20 ±

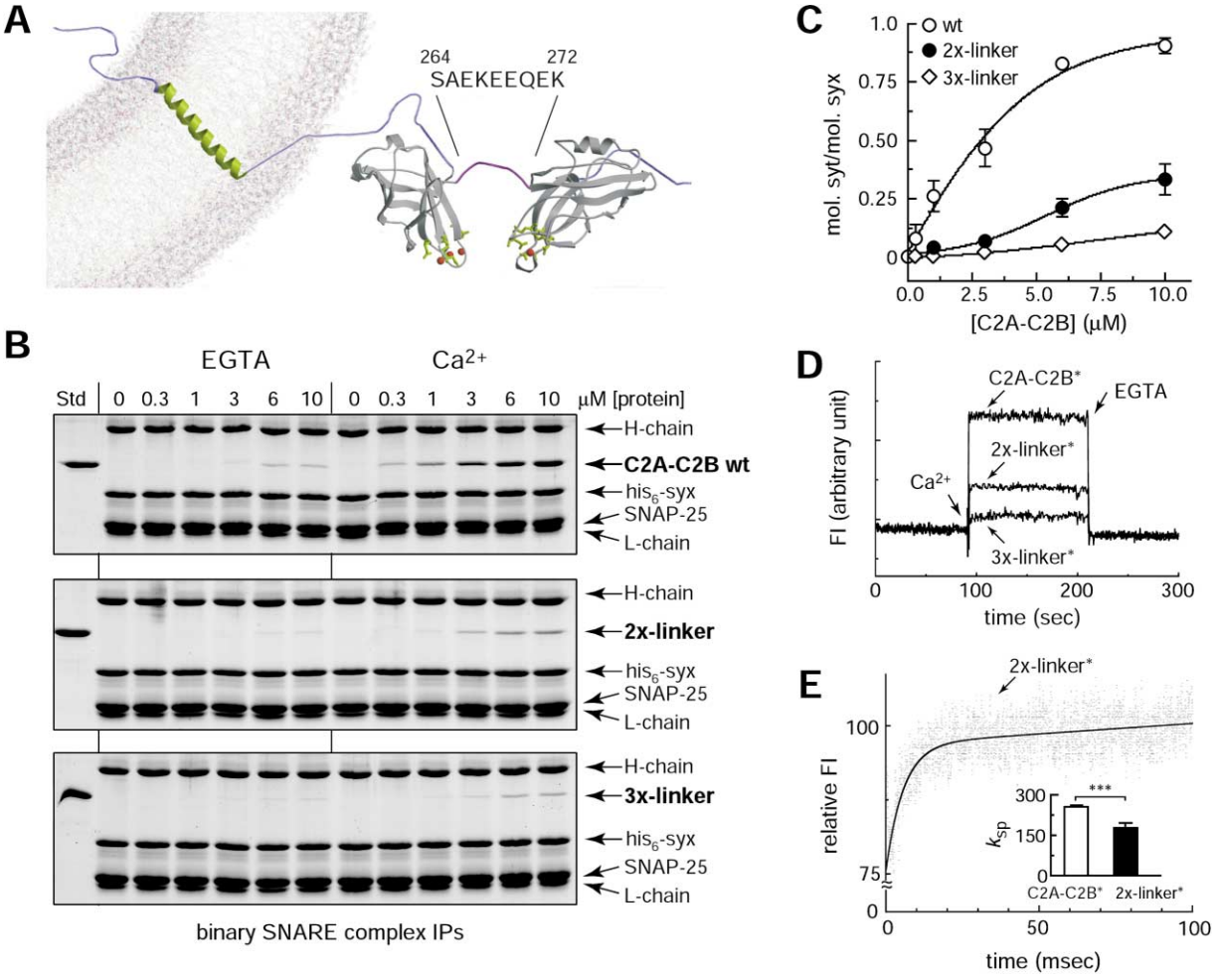

Figure 5. Lengthening the Linker that Connects C2A and C2B Disrupts syt•t-SNARE Interactions

(A) Molecular model depicting the linker region (residues 264–272) connecting C2A and C2B of syt I. The crystal structure of syt III (Sutton et al., 1999) was used as a template.

(B) Increasing the length of the C2 domain linker region reduces the t-SNARE binding activity of C2A-C2B. Two mutant versions of C2A-C2B, which have either 2 copies (designated as 2×-linker) or 3 copies (designated as 3×-linker) of the linker segment, were generated. Binding assays were carried out as described in Figure 4A; gels were stained with Coomassie blue.

(C) Ca^{2+}-triggered binding of C2A-C2B to syntaxin from (B) was quantified by densitometry and is plotted versus [C2A-C2B]. Error bars represent SD from three independent experiments.

(D) FRET experiments confirm that duplication of the linker segment disrupts SNAP-25 binding activity of C2A-C2B*. Hand mixing experiments were carried out as described in Experimental Procedures. Initially, EGTA was 0.1 mM, followed by addition of 0.6 mM Ca^{2+}; the reaction was then reversed by adding 2 mM EGTA.

(E) The linker mutations affect the rate of the slow phase of Ca^{2+}-triggered C2A-C2B*•AEDANS-SNAP-25 FRET signal change. A kinetic trace of the slow post binding component of 2×-linker*•AEDANS-SNAP-25 interactions is shown. Experiments were carried out as described in Figure 3A. 21 traces for wt and 42 traces for 2×-linker* were analyzed. The average k_{sp} values for C2A-C2B* and 2×-linker* were plotted and are shown in the inset. For C2A-C2B*, $k_{sp} = 250 \pm 6\ s^{-1}$; for 2×-linker*, $k_{sp} = 182 \pm 11\ s^{-1}$. These data indicate that the linker mutation affects a post binding rearrangement in the C2A-C2B*•AEDANS-SNAP-25 complex. ***$p < 0.001$.

2 μM, 19 ± 1 μM, and 21 ± 3 μM for wt, 2×-, and 3×-linker, respectively).

We next examined the kinetics of lipid binding by wt and linker mutant C2A-C2B. A typical kinetic trace of 3×-linker C2A-C2B•PS/PC interactions is shown in Figure 6C (left). By plotting the observed rate as a function of the [liposome] (Figure 6C, right), we obtained the k_{on}, k_{off}, and K_d for 2×-linker and 3×-linker. Wild-type and the 2×- and 3×-linker mutants exhibited identical kinetics and dissociation constants (see Figure 6C, legend).

Finally, we compared the abilities of wt and the linker mutants to bind to phosphatidylinositol 4,5-bisphosphate (PIP_2) (Schiavo et al., 1996), and the binding profiles were identical (Figure 6D).

The data above show that the linker mutations selectively disrupt syt•t-SNARE interactions but do not affect syt•membrane interactions. A number of additional putative syt•effectors have been identified (Chapman, 2002), but these binding partners interact selectively with the C2B domain of syt, which is fully functional in

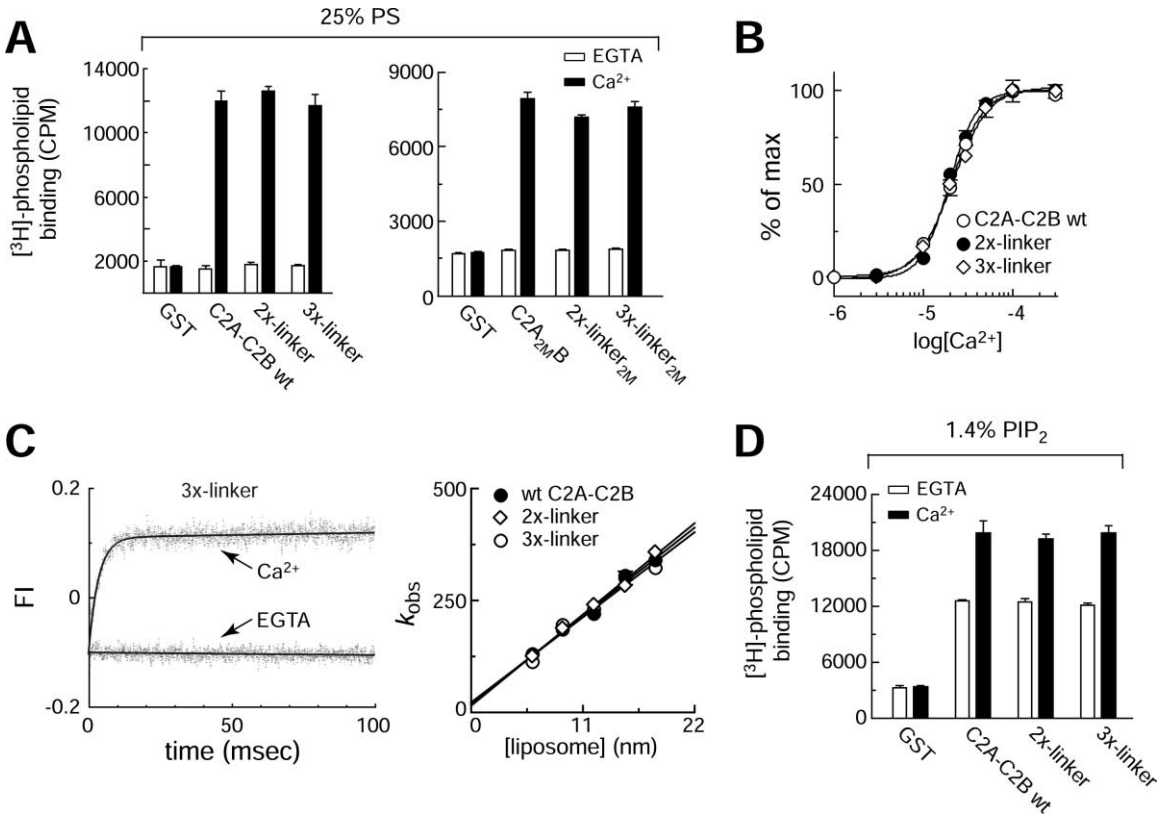

Figure 6. Lengthening the Linker that Connects the Tandem C2 Domains of syt Does Not Affect Membrane/Ca^{2+} Binding Activity

(A) Left: Wild-type, 2×-linker, and 3×-linker C2A-C2B bound the same levels of ^{3}H-labeled liposome composed of 25%PS/75%PC. Right: The Ca^{2+} and membrane binding activity of the C2A domain was disrupted by neutralization of two Ca^{2+} ligands (D230,232N) (Bai et al., 2002; Zhang et al., 1998); under these conditions, all lipid binding activity of $C2A_M$-C2B is mediated by the C2B domain. ^{3}H-labeled liposome binding assays were carried out as described (Bai et al., 2002); each construct bound identical levels of liposomes. Thus, changes in the linker do not disrupt the ability of C2A to activate the membrane binding activity of C2B (Bai et al., 2002).

(B) The linker mutations do not affect the Ca^{2+} dependence of syt•PS/PC membrane interactions. ^{3}H-labeled liposome binding assays were carried out using 25%PS/75%PC as described above, but as a function of free Ca^{2+}. Data were normalized, plotted, and fitted with GraphPad Prism 2.0 software. The $[Ca^{2+}]_{1/2}$ and Hill coefficients were: wt, 20 ± 2 μM and 2.4 ± 0.4; 2×-linker, 19 ± 1 μM and 2.8 ± 0.5; 3×-linker, 21 ± 3 μM and 2.1 ± 0.3, respectively.

(C) Stopped-flow rapid mixing experiments demonstrated that the linker mutant versions of C2A-C2B bind to PS/PC liposomes with kinetics that are identical to wt C2A-C2B. Liposomes were composed of dansyl-PE (3%), PS (25%), and PC (72%). Trp residues in wt and mutant C2A-C2B were excited at 285 nm, and the emission spectra of the dansyl-PE acceptor was collected using a 470 nm band-pass filter. Left: Representative example of the kinetics of 3×-linker•liposome interactions; a reaction carried out in Ca^{2+} (0.5 mM) is shown in the upper trace, and as a control, a mixing experiment carried out in 0.1 mM EGTA is shown in the lower trace. Right: k_{obs} values were plotted versus [liposome] to obtain k_{on} (slope) and k_{off} (*y* intercept). For wt C2A-C2B, k_{on} was 2.0 ± 0.1 × 10^{10} $M^{-1}s^{-1}$ and k_{off} was 20 ± 10 s^{-1}. Almost identical data were obtained for the 2×-linker (k_{on} was 2.0 ± 0.2 × 10^{10} $M^{-1}s^{-1}$ and k_{off} was 14 ± 11 s^{-1}) and 3×-linker versions of C2A-C2B (k_{on} was 1.9 ± 0.1 × 10^{10} $M^{-1}s^{-1}$ and k_{off} was 21 ± 17 s^{-1}). Error bars represent standard deviations (n = 3).

(D) Wild-type, 2×-linker, and 3×-linker C2A-C2B bound identical levels of ^{3}H-labeled liposome composed of 1.4%PIP_2/98.6%PC. ^{3}H-labeled liposome binding assays were carried out as described (Bai et al., 2002).

both of the linker mutants. We conclude that among known binding partners, only t-SNARE binding activity is reduced.

Acute Inhibition of Secretion from Cracked PC12 Cells Using Fragments of Wild-Type and Linker Mutant syt

In a recent study, we found that tethering two C2A domains together resulted in a single gain of function: t-SNARE binding activity (Earles et al., 2001). C2A-C2A displaces native syt from SNARE complexes in detergent extracts and rapidly inhibits exocytosis from cracked PC12 cells, potentially by blocking syt•t-SNAREs interactions during membrane fusion. Here, we further investigated the physiological role of syt•t-SNARE interactions by measuring the dominant-negative activity of the 2×- and 3×-linker versions of C2A-C2B. If syt•t-SNARE interactions are important for fusion, the linker mutations should reduce the inhibitory activity of the cytoplasmic domain of syt in cracked PC12 cells, since it will be less able to compete with native syt•t-SNARE interactions. We note that C2A-C2B could inhibit release by two other routes: competing with syt•PIP_2 (Tucker et al., 2003) and competing with syt•syt interactions (Desai et al., 2000; Tucker et al., 2003; Wu et al., 2003). To avoid inhibition mediated by these two latter ef-

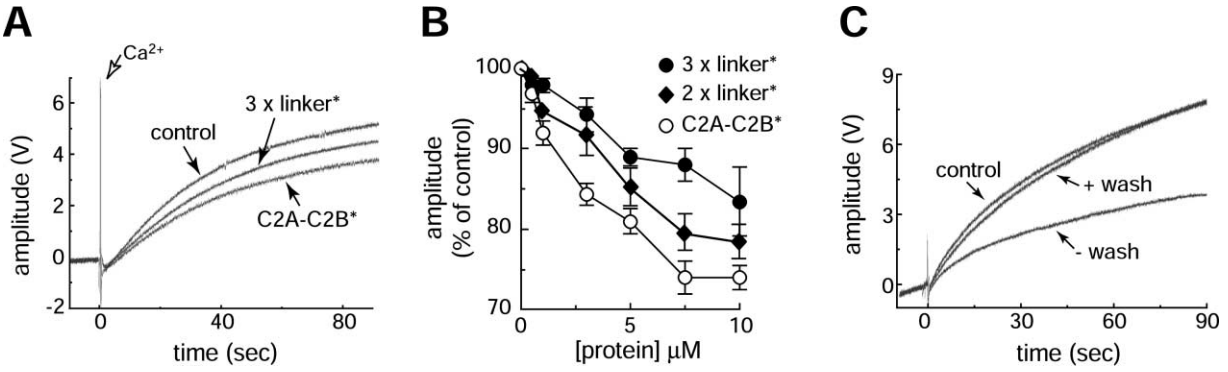

Figure 7. The Linker Mutations Abrogate the Inhibitory Activity of syt Fragments in Cracked PC12 Cell Secretion Assays

(A) Catecholamine release from PC12 cells was monitored using rotating disc electrode voltammetry as described (Earles et al., 2001). Three raw traces corresponding to the addition of HBS (control), C2A-C2B* (10 μM), or 3×-linker* (10 μM) at 1 min prior to the addition of Ca^{2+} (indicated by open arrow; 100 μM) into 350 μl of cracked cells are shown.

(B) The extent of inhibition by C2A-C2B*, 2×-, or 3×-linker* was calculated by comparing amplitudes of release profiles generated in the presence and absence of inhibitor 80 s after the addition of Ca^{2+}.

(C) The inhibitory activity of C2A-C2B washes out of cracked cells in the absence of Ca^{2+}. C2A-C2B (10 μM) was incubated with cracked cells for 10 min on ice, once set of samples were washed once in a 20-fold excess of cold release buffer; then release was triggered with Ca^{2+}. Control cells were incubated with buffer lacking C2A-C2B.

fectors, we made use of the K326,327A mutations used in the stopped-flow experiments. These mutations abrogate the inhibition caused by PIP_2 binding and oligomerization (Bai et al., 2004; Tucker et al., 2003; Wu et al., 2003). The remaining inhibitory activity is likely due to t-SNARE binding activity (Earles et al., 2001). Real-time catecholamine release profiles were obtained from cracked PC12 cells, in the presence or absence of C2A-C2B*, 2×-linker*, and 3×-linker* (Figure 7A and data not shown). The degree of inhibition was plotted versus [inhibitor] (Figure 7B), where it is evident that increasing the length of the linker that connects C2A and C2B results in a graded loss of inhibitory activity.

The inhibition data are consistent with the idea that C2A-C2B* inhibits release by blocking native syt•t-SNARE interactions during fusion. This model predicts that the ability of the cytoplasmic domain to inhibit release should be Ca^{2+} dependent; that is, the inhibitory activity of C2A-C2B should wash out of PC12 cells in the absence of Ca^{2+}. As shown in Figure 7C, when cells are incubated with C2A-C2B, and then washed prior to addition of the Ca^{2+} trigger, inhibition is no longer observed. For this experiment, we used wt C2A-C2B, demonstrating that all of the effector interactions that mediate inhibition cannot be engaged in the absence of Ca^{2+}. Thus, syt fragments inhibit release by interacting in a Ca^{2+}-dependent manner with target molecules (e.g., t-SNAREs).

Syt•t-SNAREs Interactions Regulate the Dilation Kinetics of Fusion Pores

In the final series of experiments, we expressed copies of wt and linker mutant forms of syt on the surface of secretory vesicles in PC12 cells and assessed their impact on fusion pore kinetics. In the first series of experiments, HA-tagged constructs were transfected into PC12 cells. Wild-type, 2×-, and 3×-linker were expressed at identical levels; overall syt was upregulated ~2.5-fold (Figure 8A). Transfected syts were localized by staining cells with an anti-HA antibody (Figure 8B). Each construct was efficiently targeted to large dense core vesicles (LDCV), as evidenced by the high degree of colocalization with the LDCV marker protein, secretogranin (Figures 8B and 8C; see also Supplemental Movie S1 at http://www.neuron.org/cgi/content/full/41/6/929/DC1).

Having established that wt and mutant syts were expressed at the same levels and efficiently targeted to LDCVs, we determined their impact on exocytosis. Norepinephrine (NE) release from LDCVs in transfected PC12 cells was monitored using amperometry (Figure 9A; Chow and von Ruden, 1995; Wightman et al., 1991). Release was initiated by a 6.5 s pulse of KCl. After a lag period, spikes of NE release appear, registering the fusion of vesicles and the release of their contents. Cumulative spike frequencies are plotted in Figure 9B where it is evident that the 2×- and 3×-linker mutants suppress the rate of release. Spike frequency (i.e., the maximum slopes in Figure 9B) and latencies (time from onset of stimulation to the first spike) were quantified and are plotted in Figure 9C. This analysis revealed that the observed reductions in secretion (i.e., the changes in spike frequency and the changes in release latency) were correlated with changes in the length of the linker region and with the ability of syt to engage t-SNAREs.

We then took advantage of the temporal resolution of the amperometry experiments to determine whether syt•t-SNARE interactions participate in the last steps of membrane fusion. LDCV exocytosis is usually initiated by the abrupt opening of a fusion pore with a limited conductance; subsequent expansion of the pore results in the large spikes shown in Figures 9A and 9D. Using the approach described by Wang et al. (2001), we determined the time constants of the initial open state of fusion pores—i.e., the prespike "feet." The lifetime distributions of the prespike feet from cells expressing wt, 2×-, and 3×-linker mutant syts are shown in Figure 9D.

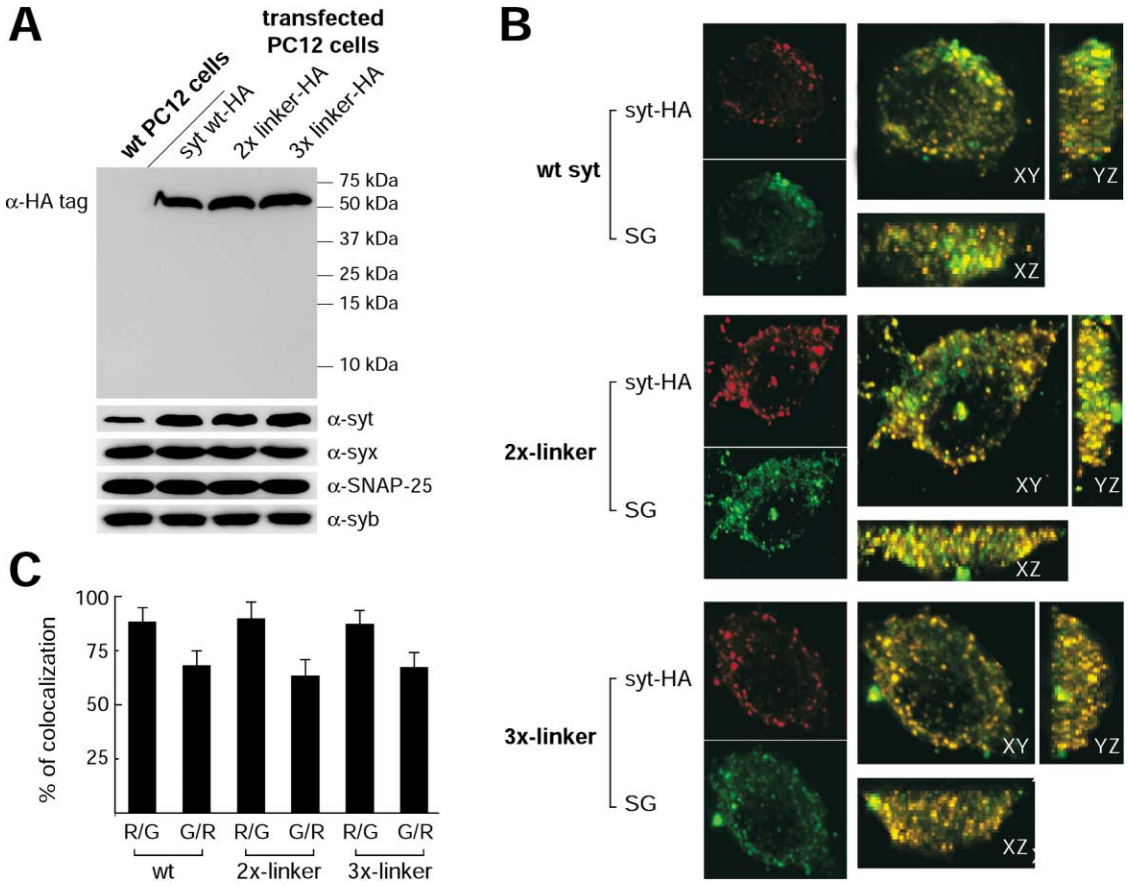

Figure 8. Expression and Targeting of HA-Tagged Wild-Type and Mutant syts in PC12 Cells

(A) Immunoblot showing HA-tagged syt expression in transfected cells (top). Bottom: Total levels of syt (endogenous and overexpressed) were assayed using and anti-syt antibody (41.1); transfection results in a ~2.5-fold increase in the level of syt. The levels of syx, SNAP-25, and syb were unaltered in transfected cells.

(B) Fluorescence localization of HA-tagged wt, 2×-, and 3×-linker syt. Cells were stained for anti-HA fluorescence (red) and for anti-secretogranin fluorescence (green). Green and red channels are shown separately on the left. 3D reconstructions of the merged images, viewed as a maximum projection from above and from two sides, are shown on the right. Yellow indicates colocalization between the two labels.

(C) Quantitation of fluorescence overlap, expressed as percentage of green (secretogranin) colocalizing with red (HA) and percentage of red colocalizing with green. HA-tagged protein was in all cases >90% colocalized with secretogranin. 60%–70% of secretogranin-labeled granules had detectable levels of HA.

The mean values of the open time from exponential fits to the fusion pore lifetime distribution were 1.65 ± 0.07 (wt), 1.33 ± 0.05 (2×-linker), and 1.01 ± 0.03 ms (3×-linker) (Figure 9E). The double-means of the prespike foot duration, computed by the method of Colliver et al. (2000), were 2.40 ± 0.19 (wt), 2.02 ± 0.20 (2×-linker), and 1.75 ± 0.15 ms (3×-linker). The difference between the wt and 3×-linker values was statistically significant, and all three values showed the same trend as the mean open times obtained by exponential fitting. Since statistical analysis of prespike foot duration indicated no significant cell-to-cell variation for this measurement (see Experimental Procedures), we can use the less conservative method based on exponential fitting to pooled events from many cells. We interpret these results as follows: upregulation of wt syt displaces copies of endogenous syt isoforms I, IX, and VII (Tucker et al., 2003) to increase the mean open lifetime of fusion pores (Wang et al., 2001). Using this as the reference point, our data reveal that graded reductions in the ability of syt to engage SNAP-25/syntaxin results in the destabilization of fusion pores.

In contrast to the prespike foot open time, the prespike foot current amplitude remained unaffected (Figure 9F), indicating that syt•t-SNARE interactions regulate the stability, but do not influence the NE permeability, of fusion pores.

Discussion

The goal of this study was to address the functional relevance of syt•t-SNARE interactions. To this end, we first investigated whether syt•t-SNARE interactions are rapid enough to couple Ca^{2+} to fusion (Hilfiker et al., 1999). Using a solution-based FRET assay, we observed that Ca^{2+} triggers the assembly of syt•SNAP-25 complexes on submillisecond timescales. Fast association is followed by a change in the FRET signal that occurs after complexes have formed, indicating that syt•SNAP-25 complexes undergo postbinding rearrange-

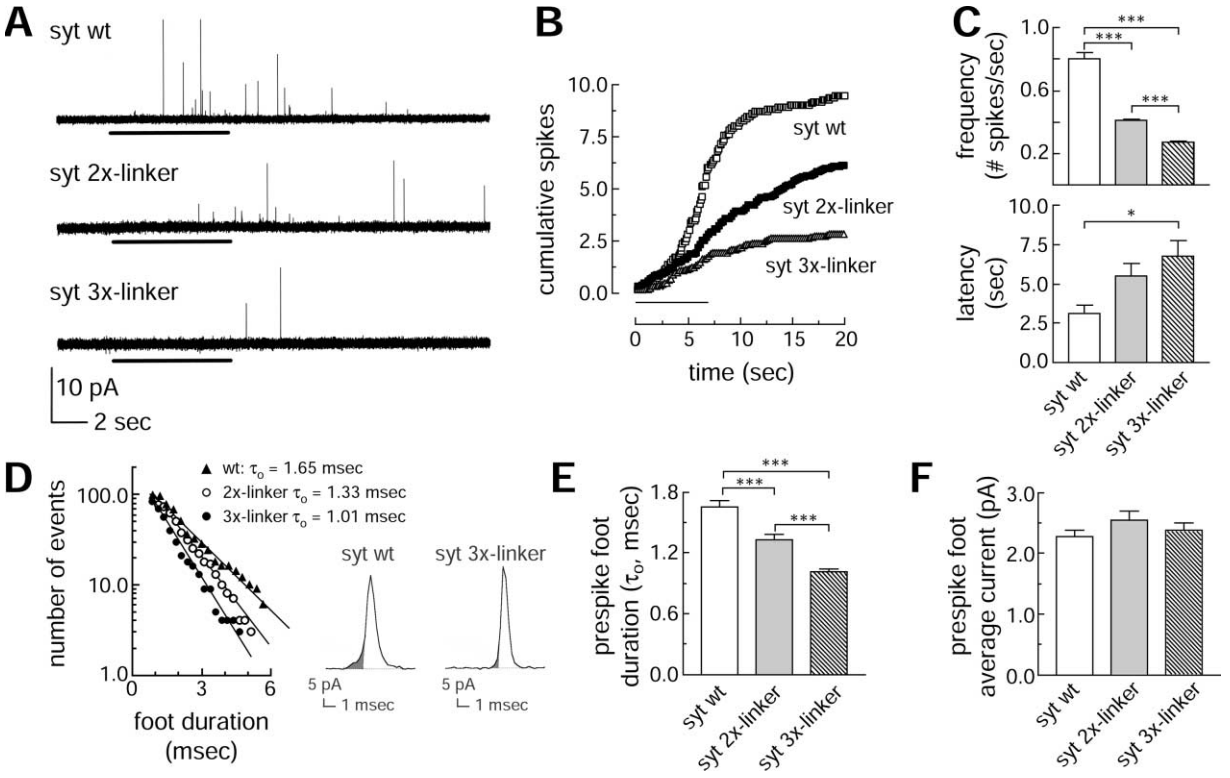

Figure 9. Loss of syt•t-SNARE Interactions Results in the Destabilization of Fusion Pores

(A) Amperometric recordings of norepinephrine release from PC12 cells transfected with full-length wt (top), 2×-linker (middle), or 3×-linker (bottom) syt. The solid bar indicates local application of 105 mM KCl for 6.5 s to depolarize the cell.

(B) Cumulative spike frequency in PC12 cells expressing wt and linker mutant versions of syt. The number of spikes per cell was averaged under each condition; the number of cells analyzed were: wt = 30, 2×-linker = 22, and 3×-linker = 22.

(C) Mean spike frequency (top) and spike latency (bottom). Frequency was calculated as the maximum slope from the plots in (B); first-spike latency was averaged from all recordings. Means are taken from the first depolarization with KCl from 22–30 cells. Each construct was transfected into cells in four independent trials. *$p < 0.05$; ***$p < 0.001$.

(D) Lifetime distribution of prespike feet from cells expressing wt, 2×-, or 3×-linker syt. Examples of amperometric spikes are shown on the right: the shaded region indicates the prespike foot signals. Single exponential fits yielded the mean open time (τ_o). τ_o was 1.65 ± 0.07, 1.33 ± 0.05, and 1.01 ± 0.03 ms for wt, 2×-, and 3×-linker syt, respectively. Data were collected from 80–99 events.

(E and F) Comparisons of τ (E) and mean NE flux (F) values obtained from PC12 cells expressing with wt, 2×-, and 3×-linker syt. ***$p < 0.001$. Note: overexpression of wt syt does not change the release frequency, latency, and average NE flux as compared to control PC12 cells that express GFP alone; the mean open time for control cells was 1.38 ms (Wang et al., 2001).

ments that result in changes in the distance and/or orientation of the donor/acceptor pair. These experiments demonstrate that Ca^{2+}-triggered syt•SNAP-25 interactions fulfill the kinetic constraints of rapid Ca^{2+}-triggered exocytosis.

Next, we determined whether syt•t-SNARE interactions function during fusion by selectively disrupting the ability of syt to engage SNAP-25 and syntaxin. We adopted a new approach in which we took advantage of the cooperation between the tandem C2 domains of syt. In all isoforms of syt described so far, C2A and C2B are connected by a linker composed of 7–9 residues (Sutton et al., 1999). While the length of the linker is conserved, its sequence is variable and it is thought to form a flexible tether. We confirmed that severing the tether strongly reduces t-SNARE binding activity and found that lengthening the linker segment resulted in graded reductions in t-SNARE binding activity. This approach differs from previous studies in which Ca^{2+} binding sites in either C2A or C2B were disrupted (Fernandez-Chacon et al., 2002; Robinson et al., 2002; Mackler et al., 2002; Stevens and Sullivan, 2003). Disruption of Ca^{2+} ligands affects a number of Ca^{2+}-triggered effector interactions, making it impossible to ascribe loss of function with loss of interaction with a defined binding partner. The linker mutations have the advantage that each C2 domain is left fully intact and able to sense Ca^{2+} in a manner identical to the wt protein—the only apparent loss of function is t-SNARE binding activity.

We expressed equivalent levels of full-length wt, 2×-, and 3×-linker mutant syts in PC12 cells, where they were efficiently targeted to LDCVs. Analysis of these cells revealed that the graded loss of syt•t-SNARE interactions results in a graded reduction in the overall rate of exocytosis. These data indicate that syt•t-SNARE interactions play a critical role in release. However, it is not clear, at this level of analysis, whether syt•t-SNARE interactions operate during the final steps of the fusion reaction, i.e., the opening and/or dilation of fusion pores.

Using amperometry, the initial open state of LDCV fusion pores can be detected as prespike foot signals in which a trickle of NE is released through pores that

have yet to dilate (Chow and von Ruden, 1995). Previous analysis of prespike feet has shown that syt can influence the stability of fusion pores (Wang et al., 2001). This work was analyzed within the framework of the following kinetic scheme:

$$\xrightarrow{k_a} C \underset{k_c}{\overset{k_o}{\rightleftharpoons}} O \xrightarrow{k_d} D.$$

C and O represent the closed and open states of the fusion pore, respectively, and D represents a dynamic state in which the fusion pore is dilating. According to this scheme, the time constant obtained from a single exponential fit to the open-state lifetime distribution can be derived as $\tau_o = 1/(k_c + k_d)$, where the rate constants correspond to the transitions indicated (Colquhoun and Hawkes, 1982; Jackson, 1992). We note that the rate of the slow rearrangement in C2A-C2B*•AEDANS-SNAP-25 complexes (Figure 3C; $\sim$250 s^{-1}) could represent one of these exit pathways.

The shorter τ_o seen with the 3×-linker mutation requires that k_c and/or k_d change in such a way that their sum increases by 40% (Figure 9D). Increasing k_c has the additional advantage of being consistent with the observed reduction in spike frequency (Figure 9C). However, a change in k_c alone is insufficient to account quantitatively for both the 3-fold decrease in spike frequency and the 40% decrease in τ_o. In order to relate the change in spike frequency to fusion pores, we note that a spike arises from an open fusion pore and the fraction of open fusion pores that produce spikes is $k_d/(k_c + k_d)$. Thus, a change in k_c alone will change τ_o and the spike frequency by the same fraction. To explain the decrease in spike frequency in excess of the reduction in τ_o, another parameter such as k_d, k_o, or k_a must change. If k_d decreases, then a large increase in k_c would be necessary to maintain the reduction in τ_o. Alternatively, if k_d remained the same, then decreases in k_o or k_a could account for the excess reduction in spike frequency. A change in k_o is appealing in its simplicity because this would confine the changes to interconversions between C and O. For example, if $k_c = k_d = 303$ s^{-1} for wt syt, then $\tau_o = 1.65$ ms. If the 3×-linker mutation increased k_c to 697 s^{-1}, this would reduce τ_o to 1 ms, as observed. The reduction in frequency of spikes would be only 40%, and the additional 2-fold reduction in spike frequency that we observed requires that k_o be reduced by this magnitude. Although other interpretations are possible, a reduction in k_o has the advantage of simplicity, as it explains two key observations in terms of transitions between the same two states. Within this kinetic framework, the selective impairment of syt•t-SNARE interactions would thus favor the closed state of the fusion pore, reducing the forward opening rate and increasing the reverse closing rate.

We propose a model in which syt binds to anionic lipids and t-SNAREs in the target membrane (Davis et al., 1999). The interaction of syt with lipids in the target membrane would facilitate SNARE complex assembly either indirectly by allowing them to zipper-up due to proximity, or via direct contacts with t-SNAREs to help drive their assembly into four-helix bundles (Littleton et al., 2001; Mahal et al., 2002). Both sets of interactions would pull the vesicle and target membranes together to initiate pore opening. In this model, the initial open state of the pore can be envisioned as being lined with the membrane anchors of synaptobrevin and syntaxin. Syt would subsequently drive the lateral separation of SNARE complexes to mediate dilation of the pore. However, whether SNAREs form fusion pores in vivo, or whether they direct the assembly or activity of other proteins that form fusion pores, has yet to be experimentally determined.

In this study, we have focused on syt isoform I and have used LDCV exocytosis from PC12 cells as a model system. A number of syt isoforms have been identified, many of which might be expressed in brain where they could shape synaptic responses (Chapman, 2002). Expression of a seizure-induced isoform, syt IV (Vician et al., 1995), has been shown to destablize LDCV fusion pores (Wang et al., 2001) in a manner similar to the syt I linker mutants described here. Consistent with these findings, upregulation of syt IV results in decreases in synaptic transmission (Littleton et al., 1999). Thus, it is tempting to speculate that different isoforms may give rise to fusion pores with distinct properties.

Experimental Procedures

DNA Constructs

cDNA encoding rat syt I (Desai et al., 2000; Perin et al., 1990), rat syntaxin 1A (Bennett et al., 1992), rat synaptobrevin II (Elferink et al., 1989), and human SNAP-25B (Bark and Wilson, 1994) were provided by T.C. Sudhof (Dallas, TX), R. Scheller (Stanford, CA), and M. Wilson (Albuquerque, NM), respectively. Syntaxin, synaptobrevin, and SNAP-25 were generated as either N-terminal his_6-tagged fusion proteins by subcloning into pTrcHis (Invitrogen) or as GST-tagged fusion proteins by subcloning into pGEX-2T (Amersham Pharmacia Biotech). The pTW34 construct for expression of full-length t-SNARE heterodimers composed of mouse his_6-SNAP-25 and rat syntaxin 1A was provided by J. Rothman and T. Weber (New York, NY) and purified by NiNTA chromatography (Parlati et al., 1999; Weber et al., 1998).

cDNA encoding the cytoplasmic domain (designated C2A-C2B, residues 96–421), the C2A domain (residues 96–265), and the C2B domain (residues 248–421) of syt were expressed as GST-tagged proteins and cleaved with thrombin as described (Desai et al., 2000).

Two mutant versions of C2A-C2B, which have either 2 (2×-linker) or 3 (3×-linker) copies of the linker sequence (residues 264–272), were generated as GST-fusion proteins as described above. For all experiments, bacterial contaminants were removed from recombinant proteins using 1 M NaCl plus RNase/DNase as described (Wu et al., 2003).

Full-length wt, 2×-linker, and 3×-linker syts were subcloned into pIRES2-EGFP vector (BD Biosciences Clontech) via EcoR I and BamH I sites. For immunolocalization and immunoblot analysis, constructs also contained the influenza hemagglutinin (HA) tag (YPYDVPDYA) placed at the C terminus of the syt inserts.

Immunoprecipitation and Antibodies

Mouse monoclonal antibodies directed against rat syntaxin (HPC-1), SNAP-25 (71.2), synaptobrevin (69.1), and syt (41.1) were provided by R. Jahn (Göttingen, GER). Mouse monoclonal antibody against the HA-tag and rabbit polyclonal antibodies directed against secretogranin were purchased from Novus Biologicals (Littleton, CO) and QED Bioscience (San Diego, CA), respectively.

SDS-resistant midi SNARE complexes (residues 180–262 of syntaxin 1A, full-length SNAP-25A, and residues 1–96 of synaptobrevin II) were provided by D. Fasshauer (Fasshauer et al., 1998) (Göttingen, Germany). Immunoprecipitation of recombinant t-SNAREs and SNARE complexes was carried out as described (Littleton et al., 2001). Briefly, SNAREs (2–3 μM) were incubated with recombinant

syt fragments (2 μM) in 150 μl Tris-buffered saline (TBS; 20 mM Tris [pH 7.4], 150 mM NaCl) plus 0.5% Triton X-100 in the presence of 2 mM EGTA or 1 mM Ca^{2+} for 1 hr. SNAREs were immunoprecipitated by mixing samples with monoclonal antibodies against syntaxin (HPC-1), SNAP-25 (71.2), or synaptobrevin (69.1) followed by addition of 40 μl Protein G Sepharose Fast-flow beads (Pharmacia). Beads were collected by centrifugation at 4000 × g for 50 s and washed four times in binding buffer, and samples were separated by SDS-PAGE; in all cases proteins were visualized by staining with Coomassie blue.

Liposomes

Brain-derived phosphatidylserine (PS), phosphatidylcholine (PC), and 1,2-dioleoyl-sn-glycero-3-phosphoethanolamine-N-(5-dimethylamino-1-naphthalenesulfulfonyl) (dansyl-PE) were obtained from Avanti Polar Lipids. L-3-phosphatidyl[*N-methyl*-^{3}H]choline-1,2-dipalmitoyl ([^{3}H]PC) was purchased from Amersham. Lipids were dried under nitrogen and suspended in HEPES-buffered saline (HBS; 50 mM HEPES [pH 7.4], 100 mM NaCl). For fluorescence studies, large (~100 nm) unilamellar liposomes were prepared using an extruder (Avanti Polar Lipids). ^{3}H-labeled liposomes were prepared by sonication using a Microson ultrasonic cell disruptor (Misonics); ^{3}H-labeled liposome binding assays were carried out as described previously (Bai et al., 2002). In all experiments, error bars represent the standard deviations from triplicate determinations.

Fluorescent Labeling of SNAP-25

Four Cys residues of SNAP-25 (residues 85, 88, 90, and 92) were labeled using a 10-fold molar excess of 1,5-IAEDANS (5-((((2-iodoacetyl)amino)ethyl)amino)naphthalene-1-sulfonic acid; Molecular Probes) using the method described previously (Bai et al., 2002). Labeled SNAP-25 (designated as AEDANS-SNAP-25) was separated from free fluorophore using Sephadex G-25 desalting columns (Amersham). The labeling stoichiometry was ~3.6 dye molecules per SNAP-25.

Fluorescence Resonance Energy Transfer Measurements

At high protein concentrations, syt•SNAP-25 complexes tend to aggregate. To avoid the turbidity that results from the precipitates, C2A-C2B harboring two mutations of K326,327A (Desai et al., 2000; designated C2A-C2B*) was used in these studies.

Steady-state fluorescence resonance energy transfer (FRET) measurements were made at 24°C using a Photon Technology International (PTI) QM-1 fluorometer and Felix software. C2A-C2B* (10 μM) and AEDANS-SNAP-25 (1 μM) were mixed in a cuvette; native tryptophan (Trp) residues in C2A-C2B* (amino acids 259, 390, and 404) served as the energy donors and were excited at 285 nm. The emission spectrum of the AEDANS-SNAP-25 acceptor was collected from 420 to 540 nm and corrected for blank, dilution, and instrument response.

Rapid-mixing FRET measurements were carried out using an Applied Photophysics SX.18MV Stopped-flow spectrometer at 25°C. Trp residues in C2A-C2B* were excited at 285 nm and the fluorescence of AEDANS-SNAP-25 was collected using a 470 nm cut-off filter. C2A-C2B* (20 μM) with 0.1 mM EGTA, and AEDANS-SNAP-25 (2 μM) with 1.1 mM Ca^{2+} were loaded into separate syringes and then rapidly mixed at a 1:1 ratio (dead time = 1.2 ms) in HBS. As a control, mixing experiments were also carried out using AEDANS-SNAP-25 in 0.1 mM EGTA instead of Ca^{2+} (lower trace), providing a minimum reference point. Data (4000 points) were collected for 100 ms and are plotted with a best-fit single exponential function.

Alternatively, stopped-flow experiments were carried out by premixing C2A-C2B*, AEDANS-SNAP-25, and EGTA (0.1 mM) in one syringe, and then rapidly mixing this sample with Ca^{2+} (0.5 mM final free [Ca^{2+}]). The kinetics traces obtained by premixing the proteins prior to mixing with Ca^{2+} were identical to the data obtained in the mixing protocol described above. Similar stopped-flow rapid mixing experiments were also used to study C2A-C2B•liposome interactions. Trp residues in 1.5 μM C2A-C2B were excited at 285 nm, and emission from dansyl-PE was collected with a 470 nm bandpass filter.

Transfections

1–2 × 10^7 cells from one 100 mm dish were transfected with 50 μg of each plasmid as described (Wang et al., 2001).

Immunocytochemistry

PC12 cells expressing HA-tagged syts (wild-type, 2×-linker, or 3×-linker) were fixed in 4% paraformaldehyde with 4% sucrose, permeabilized with 0.3% Triton X-100, and blocked with goat serum. Cells were incubated with anti-HA monoclonal antibody (1:200) followed by incubation with rabbit anti-secretogranin (1:400). The cells were then incubated with fluorescein-conjugated anti-rabbit secondary antibody (1:400) and rhodamine-conjugated anti-mouse antibodies (1:400). Cells were imaged on a Nikon TE300 inverted microscope using a 100× 1.4NA objective; images were acquired using a Micromax cooled CCD camera (Roper Scientific) controlled by Metamorph software (Universal Imaging Corp.). Z-slices were taken at 0.25 μm intervals, and the resulting Z-stacks were deconvolved and reconstructed using AutoQuant Imaging Autodeblur/autovisualize software (Watervliet, NY). Colocalization was quantified by thresholding the green and red images and measuring the overlap between the two (green to red and red to green) for each optical section.

Amperometry

Amperometry experiments were carried out as described (Wang et al., 2001). PC12 cells were depolarized with 105 mM KCl for 6.5 s using a picospritzer (General Valve Corporation); ejection pressure was 10–20 PSI. Application of KCl from the picospritzer was recorded by pClamp8 software (Axon Instruments) to precisely mark the onset of depolarization such that the latencies to the first spike could be determined. Each cell was stimulated for 1–4 consecutive trials. To acquire amperometric signals, a polarization potential (+650 mV) was applied to a freshly cut 5 μm diameter carbon fiber electrode (ALA Scientific Instruments) that was positioned to gently touch the cell. A VA-10 npi amplifier (ALA Scientific Instruments) amplified the signal, which was low-pass filtered at 1 kHz and digitized at 4 kHz by a computer running pClamp8.

Amperometry experiments were always performed on 2 or more groups of cells transfected in parallel, where one group was a control (syt I wt). This matching insured that control cells and cells transfected with mutants were handled identically so that differences could be attributed to mutations. Amperometry results were pooled from 22–30 cells and 4–6 transfections for each protein. These procedures insured that cell-to-cell variability, which has been shown to undermine analysis of spike shape with data from ≤6 cells (Colliver et al., 2000), does not compromise the analysis.

The computer program MiniAnalysis (Synaptosoft) was used to identify the amperometric spikes with amplitudes five times the RMS noise (~0.4 pA). Clampex 8 (Axon Instruments) was used to measure the latency of the first spike. Frequency and latency were taken from the first KCl trial for each cell. A program written by P.Y. Chang, in this research group, was used to determine the duration and average current of prespike feet. Prespike feet associated with spikes with amplitudes greater than 20 pA were selected. The onset of a prespike foot was taken as the time when the current departed from the baseline beyond the RMS noise. The end of a prespike foot was taken as the intersection of a line drawn through the rising phase (35%–60%) of the spike back to the baseline + RMS current (Chow and von Ruden, 1995). The prespike foot current was determined by dividing the prespike foot area by the duration. Only prespike feet ≥1 ms (more than three times of the sampling rate of 0.25 ms) were analyzed; shorter events could not be accurately measured.

Lifetime distributions of prespike feet were plotted semilogarithmically so that single exponentials appeared as straight lines. The distributions were cumulative so a value plotted represents the number of events longer than a given time. Distributions were fitted to exponentials by χ^2 minimization with computer program Origin (Microcal). The errors in parameters were determined by inversion of the covariance matrix. Single exponentials gave good fits, and adding a second exponential did not generally provide a significant improvement in the quality of the fit. The time constant obtained from a single exponential fit is equal to the mean open time of

the fusion pore. The excellent fits to single exponential functions indicate that each group contains a single population of fusion pores, which can be compared between groups of cells transfected with different proteins. Both the Kruskal-Wallis (nonparametric) test and one-way ANOVA indicated that the prespike foot has no statistically significant dependence on cell among syt I-transfected cells ($p = 0.35$ and 0.52, respectively). This indicates that, in contrast to other amperometric parameters such as spike peak amplitude and half width (Colliver et al., 2000), prespike foot duration can be pooled from different cells for analysis. When the arithmetic means of prespike foot duration were computed, they differed from the time constant of an exponential fit to the lifetime distribution by exactly the instrumental cut-off time of 0.75 ms, as expected for an exponential distribution.

All spike characteristics are reported as the mean ± standard error. One-way ANOVA with the Newman-Keuls multiple comparison test was used to evaluate statistical significance of the mean values.

Acknowledgments

We thank P. Chang for writing a computer program used to analyze amperometry data and W. Tucker, P. Wang, and A. Bhalla for discussion and comments. This study was supported by grants from the NIH (NIGMS GM 56827 and NIMH MH61876 to E.R.C. and NS30016 and NS44057 to M.B.J.) and the Milwaukee Foundation (E.R.C.). E.R.C. is a Pew Scholar in the Biomedical Sciences. J.B. is supported by an AHA postdoctoral Fellowship.

Received: April 1, 2003
Revised: January 10, 2004
Accepted: February 11, 2004
Published: March 24, 2004

References

Augustine, G.J. (2001). How does calcium trigger neurotransmitter release? Curr. Opin. Neurobiol. *11*, 320–326.

Bai, J., Wang, P., and Chapman, E.R. (2002). C2A activates a cryptic Ca^{2+}-triggered membrane penetration activity within the C2B domain of synaptotagmin I. Proc. Natl. Acad. Sci. USA *99*, 1665–1670.

Bai, J., Tucker, W.C., and Chapman, E.R. (2004). PIP_2 increases the speed of response of synaptotagmin and steers its membrane-penetration activity toward the plasma membrane. Nat. Struct. Mol. Biol. *11*, 36–44.

Bark, I.C., and Wilson, M.C. (1994). Human cDNA clones encoding two different isoforms of the nerve terminal protein SNAP-25. Gene *139*, 291–292.

Bennett, M.K., Calakos, N., and Scheller, R.H. (1992). Syntaxin: a synaptic protein implicated in docking of synaptic vesicles at presynaptic active zones. Science *257*, 255–259.

Bollmann, J.H., Sakmann, B., and Borst, J.G. (2000). Calcium sensitivity of glutamate release in a calyx-type terminal. Science *289*, 953–957.

Bommert, K., Charlton, M.P., DeBello, W.M., Chin, G.J., Betz, H., and Augustine, G.J. (1993). Inhibition of neurotransmitter release by C2-domain peptides implicates synaptotagmin in exocytosis. Nature *363*, 163–165.

Brose, N., Petrenko, A.G., Sudhof, T.C., and Jahn, R. (1992). Synaptotagmin: a calcium sensor on the synaptic vesicle surface. Science *256*, 1021–1025.

Chapman, E.R. (2002). Synaptotagmin: a Ca^{2+} sensor that triggers exocytosis? Nat. Rev. Mol. Cell Biol. *3*, 498–508.

Chapman, E.R., Hanson, P.I., An, S., and Jahn, R. (1995). Ca^{2+} regulates the interaction between synaptotagmin and syntaxin 1. J. Biol. Chem. *270*, 23667–23671.

Chapman, E.R., An, S., Edwardson, J.M., and Jahn, R. (1996). A novel function for the second C2 domain of synaptotagmin. Ca^{2+}-triggered dimerization. J. Biol. Chem. *271*, 5844–5849.

Chen, Y.A., Scales, S.J., Patel, S.M., Doung, Y.C., and Scheller, R.H. (1999). SNARE complex formation is triggered by Ca^{2+} and drives membrane fusion. Cell *97*, 165–174.

Chieregatti, E., Witkin, J.W., and Baldini, G. (2002). SNAP-25 and synaptotagmin 1 function in Ca^{2+}-dependent reversible docking of granules to the plasma membrane. Traffic *3*, 496–511.

Chow, R.H., and von Ruden, L. (1995). Electrochemical detection of secretion from single cells. In Single-Channel Recording, B. Sakmann, and E. Neher, eds. (New York, Plenum Press), pp. 245–275.

Colliver, T.L., Hess, E.J., Pothos, E.N., Sulzer, D., and Ewing, A.G. (2000). Quantitative and statistical analysis of the shape of amperometric spikes recorded from two populations of cells. J. Neurochem. *74*, 1086–1097.

Colquhoun, D., and Hawkes, A.G. (1982). On the stochastic properties of bursts of single ion channel openings and of clusters of bursts. Philos. Trans. R. Soc. Lond. B Biol. Sci. *300*, 1–59.

Davis, A.F., Bai, J., Fasshauer, D., Wolowick, M.J., Lewis, J.L., and Chapman, E.R. (1999). Kinetics of synaptotagmin responses to Ca^{2+} and assembly with the core SNARE complex onto membranes. Neuron *24*, 363–376.

Davletov, B.A., and Sudhof, T.C. (1993). A single C2 domain from synaptotagmin I is sufficient for high affinity Ca^{2+}/phospholipid binding. J. Biol. Chem. *268*, 26386–26390.

Desai, R.C., Vyas, B., Earles, C.A., Littleton, J.T., Kowalchyck, J.A., Martin, T.F., and Chapman, E.R. (2000). The C2B domain of synaptotagmin is a Ca^{2+}-sensing module essential for exocytosis. J. Cell Biol. *150*, 1125–1136.

DiAntonio, A., Parfitt, K.D., and Schwarz, T.L. (1993). Synaptic transmission persists in synaptotagmin mutants of *Drosophila*. Cell *73*, 1281–1290.

Earles, C.A., Bai, J., Wang, P., and Chapman, E.R. (2001). The tandem C2 domains of synaptotagmin contain redundant Ca^{2+} binding sites that cooperate to engage t-SNAREs and trigger exocytosis. J. Cell Biol. *154*, 1117–1123.

Elferink, L.A., Trimble, W.S., and Scheller, R.H. (1989). Two vesicle-associated membrane protein genes are differentially expressed in the rat central nervous system. J. Biol. Chem. *264*, 11061–11064.

Fasshauer, D., Eliason, W.K., Brunger, A.T., and Jahn, R. (1998). Identification of a minimal core of the synaptic SNARE complex sufficient for reversible assembly and disassembly. Biochemistry *37*, 10354–10362.

Fernandez, I., Arac, D., Ubach, J., Gerber, S.H., Shin, O., Gao, Y., Anderson, R.G., Sudhof, T.C., and Rizo, J. (2001). Three-dimensional structure of the synaptotagmin 1 C2B-domain. Synaptotagmin 1 as a phospholipid binding machine. Neuron *32*, 1057–1069.

Fernandez-Chacon, R., Konigstorfer, A., Gerber, S.H., Garcia, J., Matos, M.F., Stevens, C.F., Brose, N., Rizo, J., Rosenmund, C., and Sudhof, T.C. (2001). Synaptotagmin I functions as a calcium regulator of release probability. Nature *410*, 41–49.

Fernandez-Chacon, R., Shin, O.H., Konigstorfer, A., Matos, M.F., Meyer, A.C., Garcia, J., Gerber, S.H., Rizo, J., Sudhof, T.C., and Rosenmund, C. (2002). Structure/function analysis of Ca^{2+} binding to the C2A domain of synaptotagmin 1. J. Neurosci. *22*, 8438–8446.

Ferro-Novick, S., and Jahn, R. (1994). Vesicle fusion from yeast to man. Nature *370*, 191–193.

Fiebig, K.M., Rice, L.M., Pollock, E., and Brunger, A.T. (1999). Folding intermediates of SNARE complex assembly. Nat. Struct. Biol. *6*, 117–123.

Geppert, M., Goda, Y., Hammer, R.E., Li, C., Rosahl, T.W., Stevens, C.F., and Sudhof, T.C. (1994). Synaptotagmin I: a major Ca^{2+} sensor for transmitter release at a central synapse. Cell *79*, 717–727.

Gerona, R.R., Larsen, E.C., Kowalchyk, J.A., and Martin, T.F. (2000). The C terminus of SNAP25 is essential for Ca^{2+}-dependent binding of synaptotagmin to SNARE complexes. J. Biol. Chem. *275*, 6328–6336.

Hilfiker, S., Greengard, P., and Augustine, G.J. (1999). Coupling calcium to SNARE-mediated synaptic vesicle fusion. Nat. Neurosci. *2*, 104–106.

Jackson, M.B. (1992). Ion channels. Single-channel analysis. Methods Enzymol. *207*, 729–746.

Katz, B. (1969). The release of neural transmitter substances (Springfield, IL: Thomas).

Littleton, J.T., Stern, M., Schulze, K., Perin, M., and Bellen, H.J. (1993). Mutational analysis of *Drosophila* synaptotagmin demonstrates its essential role in Ca^{2+}-activated neurotransmitter release. Cell *74*, 1125–1134.

Littleton, J.T., Serano, T.L., Rubin, G.M., Ganetzky, B., and Chapman, E.R. (1999). Synaptic function modulated by changes in the ratio of synaptotagmin I and IV. Nature *400*, 757–760.

Littleton, J.T., Bai, J., Vyas, B., Desai, R., Baltus, A.E., Garment, M.B., Carlson, S.D., Ganetzky, B., and Chapman, E.R. (2001). Synaptotagmin mutants reveal essential functions for the C2B domain in Ca^{2+}-triggered fusion and recycling of synaptic vesicles *in vivo*. J. Neurosci. *21*, 1421–1433.

Llinas, R., Steinberg, I.Z., and Walton, K. (1981). Relationship between presynaptic calcium current and postsynaptic potential in squid giant synapse. Biophys. J. *33*, 323–351.

Mackler, J.M., Drummond, J.A., Loewen, C.A., Robinson, I.M., and Reist, N.E. (2002). The C(2)B Ca^{2+}-binding motif of synaptotagmin is required for synaptic transmission *in vivo*. Nature *418*, 340–344.

Mahal, L.K., Sequeira, S.M., Gureasko, J.M., and Sollner, T.H. (2002). Calcium-independent stimulation of membrane fusion and SNAREpin formation by synaptotagmin I. J. Cell Biol. *158*, 273–282.

Nonet, M.L., Grundahl, K., Meyer, B.J., and Rand, J.B. (1993). Synaptic function is impaired but not eliminated in *C. elegans* mutants lacking synaptotagmin. Cell *73*, 1291–1305.

Parlati, F., Weber, T., McNew, J.A., Westermann, B., Sollner, T.H., and Rothman, J.E. (1999). Rapid and efficient fusion of phospholipid vesicles by the alpha-helical core of a SNARE complex in the absence of an N-terminal regulatory domain. Proc. Natl. Acad. Sci. USA *96*, 12565–12570.

Perin, M.S., Fried, V.A., Mignery, G.A., Jahn, R., and Sudhof, T.C. (1990). Phospholipid binding by a synaptic vesicle protein homologous to the regulatory region of protein kinase C. Nature *345*, 260–263.

Rickman, C., Archer, D.A., Meunier, F.A., Craxton, M., Fukuda, M., Burgoyne, R.D., and Davletov, B. (2004). Synaptotagmin interaction with the syntaxin/SNAP-25 dimer is mediated by an evolutionarily conserved motif and is sensitive to inositol hexakisphosphate. J. Biol. Chem., in press. Published online January 6, 2004. 10.1074/jbc.M310710200.

Robinson, I.M., Ranjan, R., and Schwarz, T.L. (2002). Synaptotagmins I and IV promote transmitter release independently of Ca^{2+} binding in the C2A domain. Nature *418*, 336–340.

Rothman, J.E. (1994). Mechanisms of intracellular protein transport. Nature *372*, 55–63.

Sabatini, B.L., and Regehr, W.G. (1996). Timing of neurotransmission at fast synapses in the mammalian brain. Nature *384*, 170–172.

Schiavo, G., Gu, Q.M., Prestwich, G.D., Sollner, T.H., and Rothman, J.E. (1996). Calcium-dependent switching of the specificity of phosphoinositide binding to synaptotagmin. Proc. Natl. Acad. Sci. USA *93*, 13327–13332.

Schiavo, G., Stenbeck, G., Rothman, J.E., and Sollner, T.H. (1997). Binding of the synaptic vesicle v-SNARE, synaptotagmin, to the plasma membrane t-SNARE, SNAP-25, can explain docked vesicles at neurotoxin-treated synapses. Proc. Natl. Acad. Sci. USA *94*, 997–1001.

Schneggenburger, R., and Neher, E. (2000). Intracellular calcium dependence of transmitter release rates at a fast central synapse. Nature *406*, 889–893.

Stevens, C.F., and Sullivan, J.M. (2003). The synaptotagmin C2A domain is part of the calcium sensor controlling fast synaptic transmission. Neuron *39*, 299–308.

Sutton, R.B., Fasshauer, D., Jahn, R., and Brunger, A.T. (1998). Crystal structure of a SNARE complex involved in synaptic exocytosis at 2.4 Å resolution. Nature *395*, 347–353.

Sutton, R.B., Ernst, J.A., and Brunger, A.T. (1999). Crystal structure of the cytosolic C2A-C2B domains of synaptotagmin III. Implications for Ca^{2+}-independent snare complex interaction. J. Cell Biol. *147*, 589–598.

Tucker, W.C., Edwardson, J.M., Bai, J., Kim, H.J., Martin, T.F., and Chapman, E.R. (2003). Identification of synaptotagmin effectors via acute inhibition of secretion from cracked PC12 cells. J. Cell Biol. *162*, 199–209.

Vician, L., Lim, I.K., Ferguson, G., Tocco, G., Baudry, M., and Herschman, H.R. (1995). Synaptotagmin IV is an immediate early gene induced by depolarization in PC12 cells and in brain. Proc. Natl. Acad. Sci. USA *92*, 2164–2168.

Wang, C.T., Grishanin, R., Earles, C.A., Chang, P.Y., Martin, T.F., Chapman, E.R., and Jackson, M.B. (2001). Synaptotagmin modulation of fusion pore kinetics in regulated exocytosis of dense-core vesicles. Science *294*, 1111–1115.

Weber, T., Zemelman, B.V., McNew, J.A., Westermann, B., Gmachl, M., Parlati, F., Sollner, T.H., and Rothman, J.E. (1998). SNAREpins: minimal machinery for membrane fusion. Cell *92*, 759–772.

Wightman, R.M., Jankowski, J.A., Kennedy, R.T., Kawagoe, K.T., Schroeder, T.J., Leszczyszyn, D.J., Near, J.A., Diliberto, E.J., Jr., and Viveros, O.H. (1991). Temporally resolved catecholamine spikes correspond to single vesicle release from individual chromaffin cells. Proc. Natl. Acad. Sci. USA *88*, 10754–10758.

Wu, Y., He, Y., Bai, J., Ji, S.R., Tucker, W.C., Chapman, E.R., and Sui, S.F. (2003). Visualization of synaptotagmin I oligomers assembled onto lipid monolayers. Proc. Natl. Acad. Sci. USA *100*, 2082–2087.

Zhang, X., Rizo, J., and Sudhof, T.C. (1998). Mechanism of phospholipid binding by the C2A-domain of synaptotagmin I. Biochemistry *37*, 12395–12403.

Zhang, X., Kim-Miller, M.J., Fukuda, M., Kowalchyk, J.A., and Martin, T.F. (2002). Ca^{2+}-dependent synaptotagmin binding to SNAP-25 is essential for Ca^{2+}-triggered exocytosis. Neuron *34*, 599–611.